CFD SIMULATION OF A MESO-COMBUSTOR WITH DETAILED KINETICS

A. Frassoldati*, F. Cozzi, S. De Iuliis***, G. Riva***
alessio.frassoldati@polimi.it
*Dip. CMIC, Politecnico di Milano, P.zza Leonardo da Vinci 32– 20133 Milano
**Dip. Energia, Politecnico di Milano, Via Lambruschini 4 – 20156 Milano
***CNR – IENI (Istituto per l'Energetica e le Interfasi), Via Cozzi 53 – 20125 Milano

Abstract
Development of micro and meso scale propulsion and power-generation systems requires the capability to design mesocombustors. To this aim and to improve the understanding of flow field structure and flame stabilization in a whirl meso-combustor, a combined CFD and experimental work has been carried out.
In the present paper we present and discuss the results of the experimental activity carried out on a meso-scale whirl combustor of about 254 mm^3 in both unreactive and reactive conditions. The reactive experiments are performed at a pressure of 3 atm and using different gaseous fuels. The combustion efficiency, major species and chemiluminescent species are measured at the combustor outlet and inside the reactive volume, respectively. The meso-combustor is modeled using the CFD code Ansys-Fluent adopting a RANS approach, a 3D mesh with up to ~10^6 cells and detailed kinetic mechanisms. The comparison with measurements is satisfactory especially when the k-ω and the EDC models are adopted for describing turbulence and turbulence-chemistry interactions.

Introduction
High performance small-scale power generation and propulsion systems based on combustion are very attractive due to the high energy density of hydrocarbon fuels (~40 MJ/Kg). The development of a high efficiency small size combustor is a first step towards the design of devices able to convert chemical energy into mechanical or electrical ones. Despite these advantages, combustion in meso and micro combustor could be hindered by the high surface to volume ratio (heat losses and wall quenching issues) and by the quite short residence time (poor chemical conversion), thus a proper management and understanding of the thermo-chemical issues connected to size reduction are mandatory in order to realize operational and efficient meso-combustors.
Meso-scale combustors have been extensively studied while operating at atmospheric pressure [1-5] while few works are available at higher pressure [6]. The concept of ultra-micro gas turbine to convert the chemical energy into mechanical one has been also undertaken and demonstrated [7].

Experimental Set-up and Procedure

The AISI 321 stainless steel non-premixed meso-scale combustor is shown in Fig. 1. The cylindrical combustion chamber is 6 mm in diameter, 9 mm in length and about 254 mm^3 in volume. Swirl is generated by tangential air injection, while fuel is injected in the radial direction, at 90° with respect to the air flow. Both air and fuel injection orifices are 1 mm in diameter. The exit port is 2 mm in diameter and gases exhaust in the tangential direction, see Fig. 1. Optical access is allowed by two fused silica windows closing both end of the cylindrical combustion chamber.

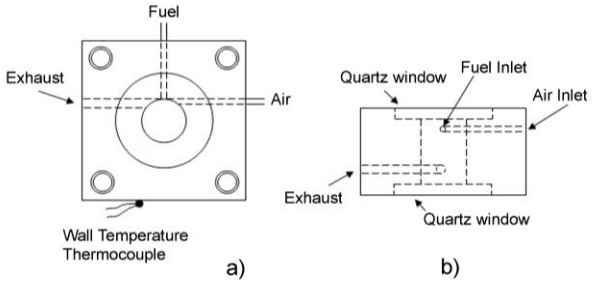

Figure 1. Meso-scale combustor: front view (a) and upper view (b)

An insulated N type thermocouple (1 mm in diameter), located in front of the exit port and at about 1 mm away from it, measures the exhaust gas temperature T_{exit}. The gas temperature was not corrected for the radiative losses. A bare wire K type thermocouple (1 mm in diameter) is used to measure the combustor wall temperature, T_{wall}.

Tests at 0.3 MPa pressure are carried out by placing the meso-combustor inside a nitrogen pressurized vessel of about 1.5 liters in volume. The desired pressure level is obtained by venting the gas through a sonic orifice.

Ambient air is used as oxidizer while methane (99.5% purity) and propane (99% purity) are used as a fuel. Fuel, oxidizer and N_2 flow rates are controlled by thermal mass flow meters (1% accuracy).

At ambient pressure and isothermal condition instantaneous two components (radial and azimuthal) single-point velocity measurements are performed in back-scattering mode by using a two-component component fiber optics Laser Doppler Velocimeter equipped with a 5 W Argon ion laser; a Bragg cell with 40 MHz frequency shift is used to remove directional ambiguity. The laser beam is conducted via glass fiber to a probe with 310 mm focal length. The size of the probe volume based on the e^{-2} intensity was about $0.09\times0.09\times0.84$ mm^{-3}. Alumina particle (diameter between 1-5 μm) dispersed into the air stream by means of cyclone were used as seeding. To compensate for the effect of velocity bias transit time weighting was applied to the estimation of both mean and RMS velocities. Five thousand (5000) velocity samples were collected at mean data rate of 50-500 Hz. The mesocombustor used for velocity measurements had the same geometry of that in Fig. 1 but the exhaust hole had a different orientation, see [8] for the detail.

Chemiluminescence measurements were carried out with an intensified CCD camera (DiCAM Pro, 12 bit) equipped with a UV-Nikon objective, and details about the experimental set-up can be found in [9].
Burned gases are sampled at the exit of the pressurized vessel for pollutant emissions analysis. A non-dispersive infrared (NDIR) analyzer is used to measure CO and CO_2 concentrations, while paramagnetic technique is used for O_2 concentration. Flame ionization detector (FID) is used to measure the total unburned hydrocarbons (TUHC).
The chemical efficiency, η_c, is estimated from the measured dry molar fractions of CO, χ_{CO}, CO_2 χ_{CO_2} and total unburned hydrocarbon TUHC, χ_{TUHC}, according to the equation $\eta_c = \chi_{CO_2} \Big/ \left(\chi_{CO_2} + \chi_{CO} + \chi_{TUHC} \right)$.

Numerical approach
3D simulation were performed under isothermal and combustion conditions by using the Fluent code. For isothermal simulations an hybrid mesh with 1.2 millions of cells has been used, permitting to minimize grid effects. Due to the high computational cost, an hybrid mesh with 130000 cells has been used under combustion conditions. This coarser mesh was tested in one reactive condition and demonstrated able to match satisfactorily the predictions obtained using the fine grid with 1.2 millions of cells.

The standard k-ω and k-ε (only for the isothermal flow cases) models were used for the description of turbulent flow, while the eddy-dissipation-concept (EDC) model was used to for the turbulence\chemistry interactions [10]. The use of EDC model assumes that reactions occur in small turbulent structures, called the fine scales. The length fraction of the fine scales is modeled as:

$$\xi^* = C_\xi \left(\nu \varepsilon / k^2 \right)^{1/4}$$

where * denotes fine-scale quantities and C_ξ is the volume fraction constant and its value is 2.1377. The volume fraction of the fine scales is calculated as ξ^{*3}. Species are assumed to react in the fine structures over a time scale

$$\tau^* = C_\tau \left(\nu / \varepsilon \right)^{1/2}$$

where C_τ is a time scale constant equal to 0.4082.
Combustion at the fine scales is assumed to occur as a constant pressure reactor, with initial conditions taken as the current species and temperature in the cell.

Reactions proceed over the time scale τ^*. The source term in the conservation equation for the mean species *i* is modeled as

$$\Omega_i = \frac{\rho\left(\xi^*\right)^2}{\tau^*\left[1-\left(\xi^*\right)^3\right]}\left(Y_i^* - Y_i\right)$$

where Y_i^* is the fine-scale species mass fraction after reacting over the time τ^*.
The kinetic schemes for methane and propane are obtained from the POLIMI complete kinetic mechanism (http://creckmodeling.chem.polimi.it/) using the reduction technique called Flux Analysis and discussed by Ceruleo [11]. These reduced mechanisms for CH_4 and C_3H_8 contain 22 and 39 species involved in 962 and 4444 reactions, respectively.
In this work, a kinetic mechanism for the species prediction has been developed considering the most important reactions of formation and consumption of OH* and CH*. This scheme was validated through the comparison of model prediction and experimental data measured in ideal reactors and laminar flames. [12]. Figure 2 shows the comparison of the predictions of the kinetic mechanism with the experimental measurements of Kathrotia et al.[13].

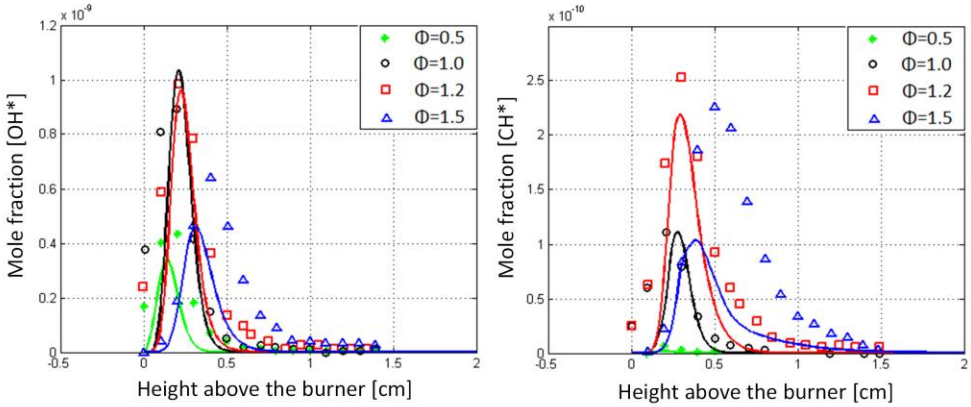

Figure 2. Comparison between predicted and measured OH* and CH* in a premixed laminar flame [13].

The P-1 model was used to consider the radiation term in the energy equation. The P-1 model is the simplest case of the more general P-N model, which is based on the expansion of the radiation intensity *i* into an orthogonal series of spherical harmonics.
The measured wall temperature was used to set the isothermal wall condition in the CFD simulations.

Table 1. Chemiluminescence sub-mechanism.

#	Reaction	A	n	E	#	Reaction	A	n	E
$R1$	$O+H+M \leftrightarrow OH^*+M$	$2.50\cdot10^{12}$	0	5972	$R11$	$C_2H+O \leftrightarrow CO+CH^*$	$1.00\cdot10^{12}$	0	0
$R2$	$CH+O_2 \leftrightarrow CO+OH^*$	$9.00\cdot10^{10}$	0	167	$R12$	$C+H+M \leftrightarrow CH^*+M$	$3.63\cdot10^{13}$	0	0
$R3$	$OH^*+N_2 \leftrightarrow OH+N_2$	$1.08\cdot10^{11}$	0.5	−1238	$R13$	$CH^*+N_2 \leftrightarrow CH+N_2$	$3.03\cdot10^{2}$	3.4	−381
$R4$	$OH^*+O_2 \leftrightarrow OH+O_2$	$2.10\cdot10^{12}$	0.5	−482	$R14$	$CH^*+O_2 \leftrightarrow CH+O_2$	$2.48\cdot10^{6}$	2.14	−1720
$R5$	$OH^*+H_2O \leftrightarrow OH+H_2O$	$5.92\cdot10^{12}$	0.5	−861	$R15$	$CH^*+H_2O \leftrightarrow CH+H_2O$	$5.3\cdot10^{13}$	0	−0
$R6$	$OH^*+H_2 \leftrightarrow OH+H_2$	$2.95\cdot10^{12}$	0.5	−444	$R16$	$CH^*+H_2 \leftrightarrow CH+H_2$	$1.47\cdot10^{14}$	0	1361
$R7$	$OH^*+CO_2 \leftrightarrow OH+CO_2$	$2.75\cdot10^{12}$	0.5	−968	$R17$	$CH^*+CO_2 \leftrightarrow CH+CO_2$	0.241	4.3	−1694
$R8$	$OH^*+CO \leftrightarrow OH+CO$	$3.23\cdot10^{12}$	0.5	−787	$R18$	$CH^*+CO \leftrightarrow CH+CO$	$2.44\cdot10^{12}$	0.5	0
$R9$	$OH^*+CH_4 \leftrightarrow OH+CH_4$	$3.36\cdot10^{12}$	0.5	−635	$R19$	$CH^*+CH_4 \leftrightarrow CH+CH_4$	$1.73\cdot10^{13}$	0.5	167
$R10$	$OH^* \rightarrow OH+h\nu$	$1.45\cdot10^{6}$	0	0	$R20$	$CH^* \rightarrow CH+h\nu$	$1.86\cdot10^{6}$	0	0

Results and discussion

Figure 3 shows a sketch of the device used for the cold flow experiments. Five different planes were used for the LDV experimental measurements. Some of the results are summarized in figure 4.

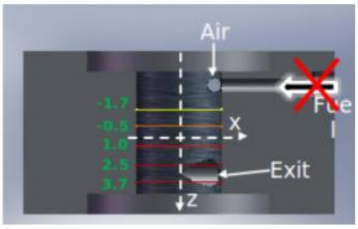

Figure 3. Cut-view of the meso-combustor showing the location of the five planes for LDV measurements.

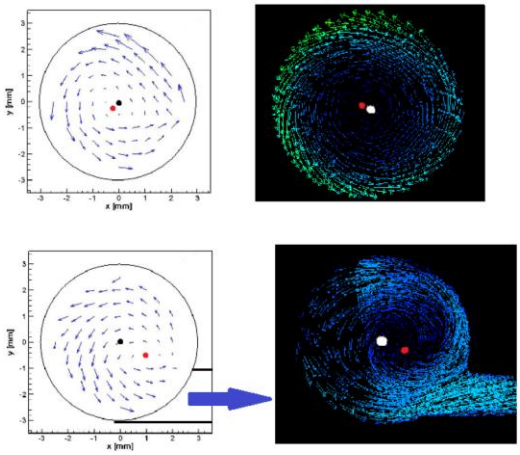

Figure 4. Measured (left) and computed velocity (right) field. Upper figure plane at x= -1.7 mm, lower figure plane at x=3.7 mm. Location of the vortex center is shown by the red dot.

It is possible to observe the presence of a vortex structure, and the complex behavior of the vortex centre. The right side of Fig. 4 shows the predicted values,

while the left side shows the flow field measured by LDV technique. Moving along the vertical coordinate, the vortex centre not only rotates around the axis, but also oscillates around the geometrical centre of the chamber as depicted in Fig. 5. A maximum distance from the geometrical centre is observed experimentally at vertical coordinates of about z=-0.5 and z=4 mm (close to the outlet). It is possible to observe that only the k-ω turbulence model is able to accurately describe this complex behavior. Nevertheless, the comparison is less satisfactory when the angular position is considered. Both turbulence models partially fail in predicting the angular position of the vortex in the region z=1÷2 mm.

Figure 6 completes the analysis of the isothermal case. Measured tangential velocities are compared to model predictions obtained with the two turbulence models. It is possible to notice that both models correctly captured the variation (decrease rate) of the tangential velocities moving along the vertical coordinate following two lines (#1 and #2) parallel to the chamber axis.

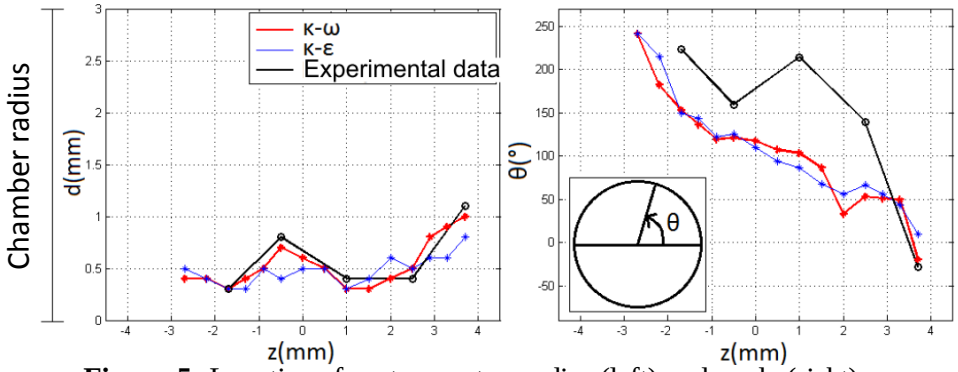

Figure 5. Location of vortex center, radius (left) and angle (right).

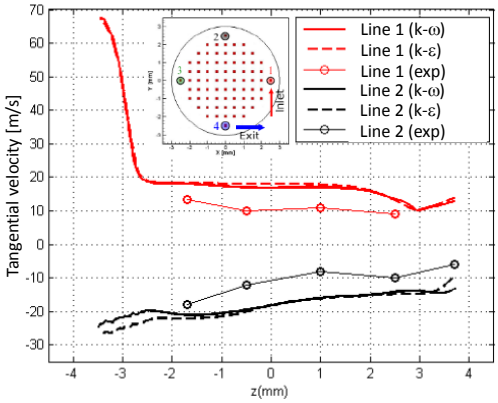

Figure 6. Measured (empty symbol) and computed (lines) tangential velocity along two lines parallel to the chamber axis. The position of line #1 and #2 in an horizontal plane is also illustrated.

CFD Results – Combustion

This paragraph illustrates the comparison between model predictions and measurements in the case of a reactive condition. A total mass flow rate of $2.08*10^{-4}$ kg/s at different equivalence ratios are considered for a CH4/air mixture. Figures 7 and 8 compare experimental and numerical results for exit temperature, mole fraction of CO and combustion efficiency.

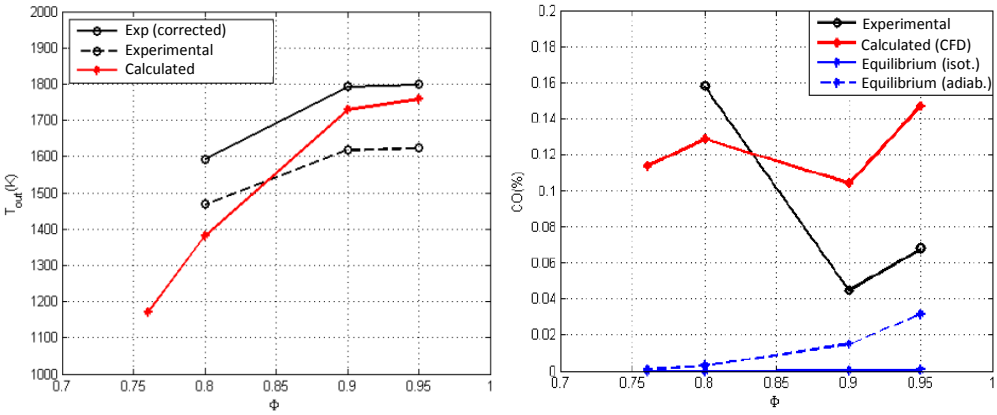

Figure 7 Gas temperature (left), and CO concentration (right) at the exhaust. Solid black line (left figure) is the measured temperature corrected for radiative heat losses.

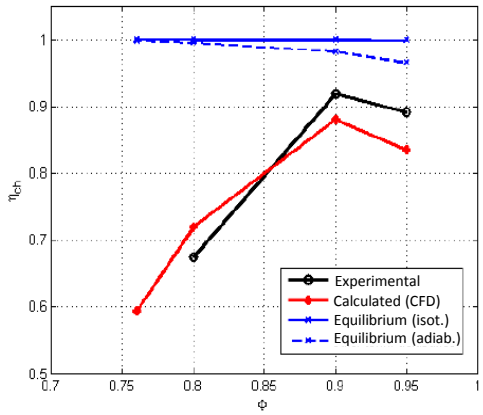

Figure 8. Computed and measured chemical efficiency.

To underline the importance of fluid dynamic and chemical kinetic in limiting the overall combustion efficiency, both adiabatic and isothermal chemical equilibrium computations has been also carried out. The decrease of computed CO concentration and the increase of UHC (the latter not shown here) observed

between Φ =0.8 and Φ =0.76 is likely due to approaching the lower stability limit. The latter results from CFD simulation to be at about Φ =0.7 and agree quite well the experimental value of 0.71. About chemical efficiency, the maximum is observed at Φ =0.9 and it decreases quickly for lean mixtures. As expected, the simple chemical equilibrium computation doesn't allows a correct prediction of species concentration and chemical efficiency.

Chemiluminescence in the meso-scale combustor.

For experimental and numerical tests about chemiluminescence a total mass flow rate of $6.19*10^{-5}$ kg/s at Φ=1 has been considered. Both experimental and numerical results, see Fig. 9, show the presence of OH* and CH* in the low chamber side, at some distance from the wall. The experimental results are shown in a.u., while numerical ones are the mole fractions of the excited specie thus a quantitative comparison between the two cannot be made. Nevertheless the qualitative agreement is satisfactory and indicates that the models used in the CFD code (kinetic mechanism, turbulence chemistry interaction, turbulence model) are able to correctly identify the region where the larger heat release rate is located.

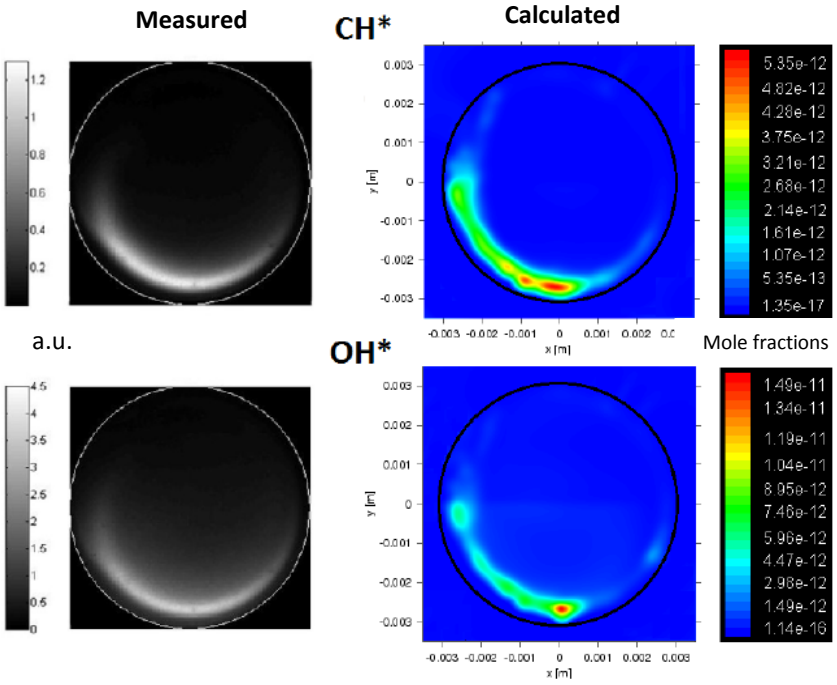

Figure 9. Measured (left) [9] and calculated (right) 2D radical chemiluminescence imaging at Φ=1.

Conclusions

A combined CFD and experimental work on a meso-scale whirl combustor has been carried out. Both isothermal and combustion conditions have been investigated.
Under isothermal condition the numerical flow field obtained from RANS simulation and standard k-ω model resulted in quite good agreement with the experimental one. Likely due to the better performance for wall-bounded and low Reynolds number flows the results for k-ω model appears to be better than the standard k-ε.
The lean combustion limit, the chemical efficiency and the exhaust gas composition were computed using standard k-ω and EDC combustion models, despite the quite coarse grid size, a satisfactory agreement was achieved with the experimental results.
A kinetic scheme has been developed for the CH* and OH* chemiluminescence, and used for the combustion simulation. The computed location of the highest CH* and OH* concentration match quite well with the experimental location of the maximum chemiluminescence emission.
The results evidence that the combined approach of CFD simulation and experimental analysis could allow a better understanding of the flow field structure and flame stabilization in the whirl meso-combustor.

References

[1] Ju, Y., Maruta, K., "Microscale combustion: technology development and fundamental research", *Prog. Energy Combust. Sci.*, 37:669–715 (2011).
[2] Maruta, K., Micro and mesoscale combustion. *Proc. Combust. Instit.* 33:125-150 (2011).
[3] Kaisare, N.S., Vlachos, D.G.,"A review on microcombustion: fundamentals, devices and applications", *Prog. Energy Combust. Sci.*, 38:321–359 (2012).
[4] Wu, M., Wang, Y., Yang, V., Yetter R.A.,"Combustion in meso-scale vortex chambers", *Proc. Combust. Instit.* 31:1265-1272 (2006).
[5] Cozzi, F., Coghe, A., Olivani, A.,"Thermal and chemical efficiencies of a meso-scale combustor for propulsive or power generation systems", *Third International Conference on Green Propellants for Space Propulsion*, Poitiers, France, pp. 1-6 (2006).
[6] Cozzi, F., De Iuliis, S. Capelli, F., Coghe, A., "Performances of a mesocombustor at 0.3 MPa with preheated air ", the 35th Meeting of The Italian Section of The Combustion Institute, Milan, Italy, paper VII-4, pp. 1-6 (2012).
[7] Tanaka S, Hikichi K, Togo, S., Murayama M, Hirose Y, Sakurai T, et al., "World's smallest gas turbine establishing Brayton cycle", *the 7th international workshop on micro and nanotechnology for power generation and energy conversion applications* (Power MEMS 2007), pp 359-362 2007.
[8] Cozzi, F., Coghe, A., D'Angelo, Y., Renou, B., Boukhalfa, M., "Experimental study of performances and internal flow field of a meso-scale vortex-combustor", *the 4th European Meeting on Combustion*, Vienna, Austria, paper 810-358 pp.1-6 (2009).

[9] De Iuliis, S., Giassi, D., Maffi, S., Cozzi, F., Dondè, R., ”Chemiluminescence measurements in a meso-scale combustor fueled with CH4/air at 0.3 MPa”, *the 35th Meeting of The Italian Section of The Combustion Institute*, Milan, Italy, paper II-3, pp. 1-6 (2012).

[10] Magnussen, B. F. “On the structure of turbulence and a generalized eddy dissipation concept for chemical reaction in turbulent flow”. 19th AIAA Aerospace Science Meeting, St. Louis, MO, 1981.

[11] Ceruleo, V., “Metodi di riduzione di schemi cinetici dettagliati”, Ms Thesis, Politecnico di Milano (2011).

[12] Riva, G., “Simulazione RANS con schemi cinetici dettagliati di un meso-combustore in pressione”, Ms Thesis, Politecnico di Milano (2013).

[13] Kathrotia, T. , Riedel, U. ,· Seipel, A., Moshammer,· K. , Brockhinke, A., “Experimental and numerical study of chemiluminescent species in low-pressure flames”, Appl. Phys. B. 107:571–584 (2012)